UNIVERSITY OF BIRMINGHAM

Kinematic HAADF-STEM image simulation of small nanoparticles

He, Dongsheng; Li, Ziyou; Yuan, J.

Document Version
Publisher's PDF, also known as Version of record

Publisher Rights Statement:
Eligibility for repository : checked 19/05/2015

Kinematic HAADF-STEM image simulation of small nanoparticles

D.S. He [a],[**], Z.Y. Li [a],[*], J. Yuan [b]

[a] Nanoscale Physics Research Laboratory, School of Physics and Astronomy, University of Birmingham, Edgbaston, Birmingham B15 2TT, UK
[b] Department of Physics, University of York, Heslington, York YO10 5DD, UK

ARTICLE INFO

ABSTRACT

The high-angle annular dark field-scanning transmission electron microscopy (HAADF-STEM) has been widely used in nanoparticle characterization due to its relatively straightforward interpretability, although multislice simulation is often required in order to take into account the strong dynamical screening effect if quantitative structure information is needed. The multislice simulation is very time-consuming, which can be a hurdle in cases when one has to deal with a large set of images. In this paper, we introduce a simple computer program, based on kinematic-scattering method, which allows users to simulate HAADF-STEM images of small nanoparticles, in 'real time' on a standard desktop computer. By comparing with the sophisticated multislice simulation, we demonstrate that such an approach is adequate for nanoparticles of ~3 nm in diameter (assuming an approximately spherical shape), particularly away from strict zone axis conditions. As an application, we show that the efficient kinematic simulation allows quick identification of orientation of nanoparticles.

1. Introduction

The high-angle annular dark field scanning transmission electron microscopy (HAADF-STEM) is one of the high-resolution electron microscopy techniques that benefits most from the recent technical improvement of the aberration corrector (Haider et al., 1998), pushing the lateral resolution reliably to sub Angstrom (Nellist et al., 2004). As a result, the HAADF-STEM technique has attracted enormous attention for its applications in tomography (Van Aert et al., 2011; Scott et al., 2012), size/mass/thickness measurement at atomic scale (Han et al., 2012; Young et al., 2008; Katz-Boon et al., 2013), structure characterization (Li et al., 2008; Chen et al., 2013) and composition measurement (Kauko et al., 2012). Differing from the conventional transmission electron microscopy (CTEM), where the specimen is illuminated by a (nearly) parallel broad beam (Wang, 2000), HAADF-STEM uses a sharply focused beam to scan across the specimen and the annular dark field (ADF) detector collects only the scattered electrons. The resulting image contrast is often referred as Z-contrast. This is because, to the first order approximation, the electron scattering can be considered in analogy with Rutherford scattering, where the scattering cross section is proportional to Z^n in which Z is the atomic number of the element in study and the power exponent n is around 1.7 (Wang et al., 2011).

The highly localized interaction between the electron beam and the specimen leads to the formation of the transversal incoherent image by collecting either the dynamically scattered coherent electrons or thermally scattering electrons (Nellist and Pennycook, 1999; Jesson and Pennycook, 1995) as long as the collection angle of the HAADF detector is large enough (approximately three times larger than the convergence angle; Hartel et al., 1996). This imaging mode has the advantage of the direct interpretation with no contrast reversal issues with changes of defocus condition, a problem in CTEM (Nellist and Pennycook, 2000). However, quantitative understanding of the image intensity for each pixel, which is often expressed as a percentage of the incident beam (LeBeau et al., 2008), is not a trivial task and simulation is usually needed. One of the most widely used image simulation methods is the multislice simulation (Kirkland, 2010) that considers both the dynamically scattered electrons and thermally scattered electrons. In this simulation, the specimen is sectioned into slices, the electron beam is modified by the atomic potential in each slice and the modified wave propagates in the free-space within the slice. The resulting scattered intensities are then integrated over the detector area and the result is evaluated pixel by pixel. The multislice simulation of the STEM image formation is inherently slow. Currently, there are several sophisticated open-sources (Koch, 2002; Galindo et al., 2008;

* Corresponding author. Present address: Center of Advanced Nanocatalysis and School of Chemistry and Materials Science, University of Science and Technology of China, Hefei, Anhui 230026, PR China.
** Corresponding author.
E-mail addresses: dshe@ustc.edu.cn (D.S. He), z.li@bham.ac.uk (Z.Y. Li).

Grillo and Rotunno, 2013) or commercially available STEM software (HREM). However, the time required to complete each simulation is usually an issue, in particular, when a desktop computer is used (Dwyer, 2010). Today, the advancement of sophisticated microscopes has already enabled very fast image acquisition, for example, a few seconds or less per image. The increasingly wide availability of the state-of-art HAADF-STEM means that the image simulation is, in many cases, now the bottleneck for understanding the three dimensional structure of nanoparticles. This is especially problematic in the case of studying the dynamic behavior of nanoparticles where usually a large number of images of the nanoparticles are required and their interpretation requires comparison of the image simulation with the suitable model atomic structures. This is a time-consuming process and especially so for many researchers who have limited access to supercomputing facilities. However, it has been demonstrated experimentally that the electron scattering can be approximated by kinematic scattering for atomic columns less than 10–50 atoms (Young et al., 2008; Li et al., 2008; LeBeau et al., 2010; Van Aert et al., 2013), depending on the orientation of nanoparticles to the electron beam and electron mean free paths in the materials. The assumption of kinematical scattering significantly simplifies the calculation involved, as the intensity-thickness relation can be treated as a linear function.

In this work, we introduce a kinematic-model-based method (Curley et al., 2007), which accelerates the HAADF-STEM simulation to achieve nearly 'real time' simulation on an Intel CPU with a clock speed of 3.2 GHz (380 MGFLOPS), for isolated nanoparticles containing less than 1000 atoms (~3 nm in diameter, assuming an approximately spherical shape). The equivalent thickness of 3 nm should be applied for nanoparticles of other shape. The software is written in Matlab 7.12.0.635 (R2011a) and a Graphic User Interface (GUI) has been incorporated to ease the steps of imaging parameter optimization. In this paper, the basic mathematical description of the simulation is introduced and several illustrative examples are presented. For small crystalline nanoparticles, the simulation can be used to compare experimental and model images once a scaling factor has been identified. For large particles, the simulation can provide a qualitative intensity variation pattern which is particularly useful in distinguishing nanoparticle orientation, and can be used as a starting point for a full multislice simulation. The software package is available as a stand-alone code, free on request by contacting the corresponding authors of this paper.

2. Mathematic model of kinematic simulation

In kinematic scattering, each electron is only scattered once, thus the number of scattered electrons is proportional to the number of atoms along their propagation direction. In this regard, the intensity at each point can be viewed as a linear addition of the contribution from each atom, i.e.

$$I_{\text{image}} = \sum_i I_{\text{atom}}(i), \tag{1}$$

where $I_{\text{atom}}(i)$ is the intensity contribution of the ith atom, which is described by

$$I_{\text{atom}}(i) = Z^n \exp\left(-\frac{d_i^2}{2c_g^2}\right), \tag{2}$$

where Z, n, c_g and d_i are the atomic number of the ith atom, the power exponent, the Gaussian factor and the distance between the ith atom and the position is concerned, respectively. Z^n describes the departure of scattering cross-section to the ideal Rutherford scattering, where $n = 2$. Depending on the collection angle of the

detector, n is usually between 1.5 and 1.8 (Wang et al., 2011; Hartel et al., 1996). c_g is the Gaussian factor that describes the effective width of the probe, which also includes the effect of aberrations, defocus as well as the incoherence (energy spread) of the illuminating electron beam.

The orientation of nanoparticles with respect to the direction of the incident electron beam can be obtained by rotating the structural model, this is done by matrix multiplication. The coordinates of atoms in the structural model are described in three columns [C_x, C_y, C_z]. The rotation of the coordinates of the atoms can be realized by multiplying with three matrixes,

$$R_x = \begin{bmatrix} 1 & 0 & 0 \\ 0 & \cos\alpha & \sin\alpha \\ 0 & -\sin\alpha & \cos\alpha \end{bmatrix}, \tag{3}$$

$$R_y = \begin{bmatrix} \cos\beta & 0 & -\sin\beta \\ 0 & 1 & 0 \\ 0 & \sin\beta & \cos\beta \end{bmatrix}, \tag{4}$$

$$R_z = \begin{bmatrix} \cos\gamma & \sin\gamma & 0 \\ -\sin\gamma & \cos\gamma & 0 \\ 0 & 0 & 1 \end{bmatrix}, \tag{5}$$

where α, β and γ are the angles rotating around x-, y- and z-axis. In principle, any orientation can be uniquely defined by two rotation parameters. Here three orientation angles are provided for the ease of interactive manipulation. The rotated atomic coordinates are $(R_z R_y R_x([C_x, C_y, C_z]^T))^T$, where the superscript T is the transportation of the matrix, meaning the model rotates around x-, y- and z-axis in that particular order. The rotation is referred with respect to the axis of the frame of references and not to any direction embedded within the model itself (the extrinsic rotation; Arfken, 1985). After the rotation, the coordinates representing the position along the z-axis are discarded as the simulation is only performed for the 2D structure projected at the x–y plane using the Eqs. (1) and (2).

3. Design of the software

Fig. 1(a) is the flowchart showing how the software works, and Fig. 1(b) is a screen shot of the layout of the software. The atomic coordinates can be imported using either .xyz or .txt files. For direct visual comparison, the experimental image can be displayed on the screen side-by-side with the simulated image and the hardball model. By making use of the DM3 input plug-in (Koch, 2002), the software accepts the experimental images in DM3 file format acquired by widely used Gatan's Digital Micrograph software. Once the experimental image is imported, the fast Fourier transform (FFT) of the image is displayed automatically.

In this software, the following parameters can be optimized: image size, X and Y offset, exponent number for the Z-contrast, Gaussian broadening parameters and orientations. The image size can be adjusted by image width in Angstrom and the pixel number in the simulation. The image width only controls the region that is displayed while reducing the pixel number used can reduce the calculation time. The simulation image is centered with the mean atomic coordinates at X and Y directions, which may cause the region of interest to be outside the display range. In such cases, X and Y offset can be used to move the simulation image. The power exponent, n, can be adjusted to take into account of the microscope operating parameters (Wang et al., 2011; Hartel et al., 1996). Increasing or decreasing n is correlated with the inner angle of the ADF detector and has the effect of changing the image contrast. The maximum n value is set to 2, although the exact value of n is best determined by the fitting of HAADF-STEM images of a
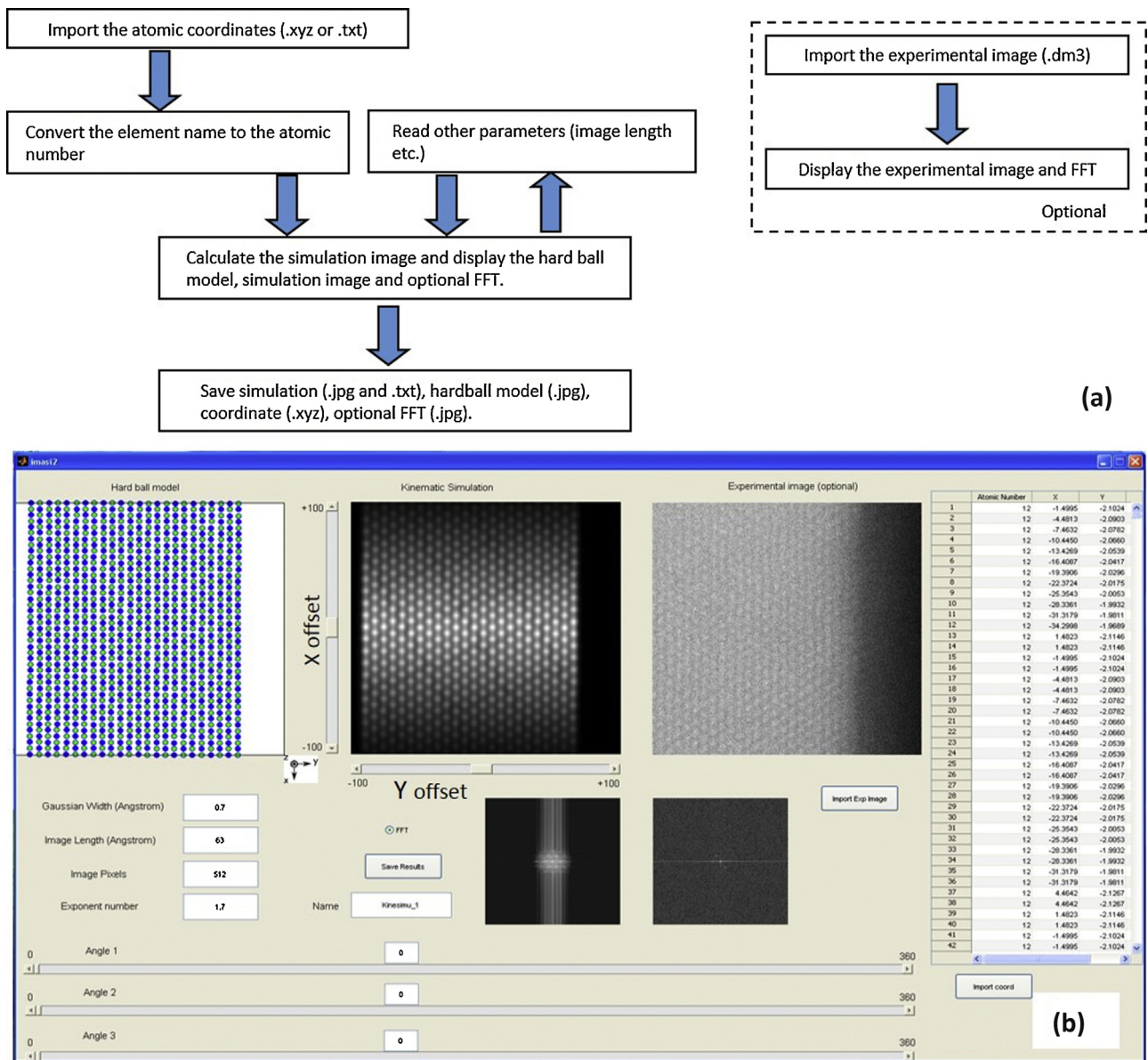
Fig. 1. Flowchart (a) and screen shot (b) of the software. The Angle 1, 2 and 3 is the same as α, β and γ as defined in the text. The experiment image and the simulation are for MgO along the $\langle 0\,1\,1 \rangle$ zone axis.

nanoparticle with a known structure. The Gaussian width, i.e. c_g in Eq. (2), can be adjusted by the user, to be consistent with spatial resolution of the images, which is a measure of the effective probe size at the time when the images are acquired. The sample orientation is controlled by the slide bars for the three rotation angles, Angle 1, 2 and 3 which is α, β and γ in Eqs. (3)–(5), respectively. For each orientation angle, it ranges from 0° to 360° to provide the ability to explore all possible orientations. All the orientation parameters controlled by the slide bars can also be viewed by digital numerical displays. This allows the user to have the parameters to repeat their simulations easily at later stage if they wish. The hard-ball model of the nanoparticles used for STEM simulation at a desired orientation is also displayed alongside the simulation. There is an option to show the FFT in real time. The simulation is saved as a text image to enable further adjustment (such as brightness, contrast, or the colormap) using other softwares such as ImageJ. The new atomic coordinates (.xyz) of the nanoparticles in the new orientation is generated and saved such that they can be exported for further multislice simulation.

4. Case studies

4.1. Kinematic simulation vs. multi-slice simulation

4.1.1. Crystalline structure

Fig. 2 shows the comparison between the kinematic simulation and the multislice simulation based on an isolated truncated octahedral cluster with 861 gold atoms. This is a magic number cluster having a complete outer shell (Martin, 1996). Unlike the multislice simulation, which has a unit for each value, i.e. a percentage of the incident beam intensity, the unit of the simulation images generated by the present software is arbitrary, so only relative intensity variation is of significance unless the image intensity is calibrated (LeBeau et al., 2008, 2010; He and Li, 2014; Nellist et al., 2010).

Fig. 2(b) shows a 512 × 512 pixels STEM image of Au_{861} cluster generated from multislice simulation using QSTEM (Koch, 2002). Here, 15 layers of slicing were employed. Other parameters are listed in Table 1. It took 2 days to complete this simulation on an Intel CPU with clock speed of 2.67 GHz. A larger number of slices
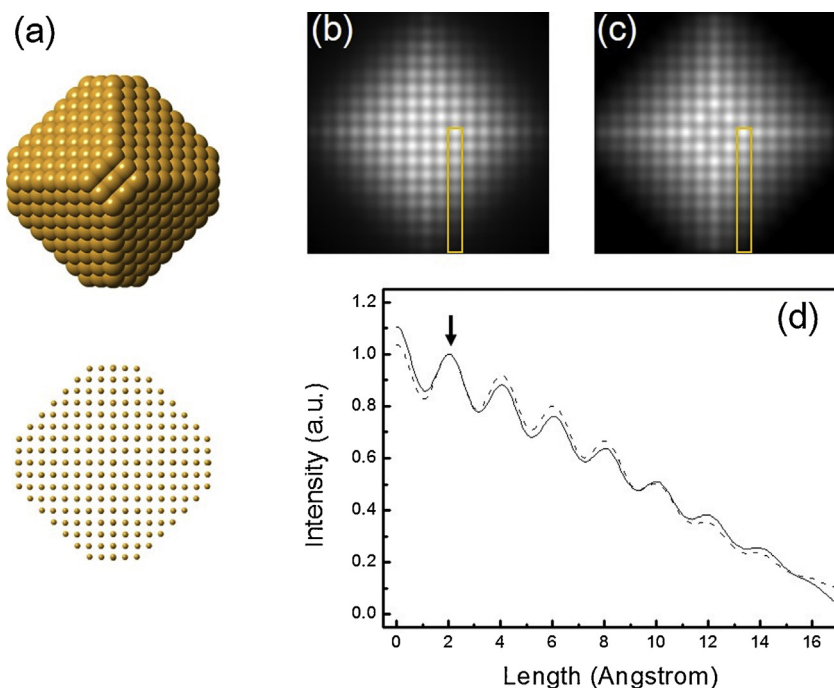
Fig. 2. Intensity comparison between multislice simulation and kinematic simulation of a truncated octahedral Au cluster with 861 atoms (a). (b) Multislice simulation generated from Q-STEM; (c) kinematic simulation generated from the software described in the present paper. The image length of (b) and (c) is 3.4 nm. (d) Line profiles of the marked yellow bars (15 pixels in width) in (b) (dashed line) and (c) (solid line). (For interpretation of the references to color in this figure legend, the reader is referred to the web version of this article.)

Table 1
Multislice simulation parameters.

Parameter	Value
Convergence angle (k_0)	15 mrad (5.45 nm^{-1})
Inner collection angle (k_1)	60 mrad (21.82 nm^{-1})
Outer collection angle (k_2)	160 mrad (58.18 nm^{-1})
Defocus	−61.3 nm
Spherical aberration	1 mm
Chromatic C	1 mm
ΔE	0.6 eV
Accelerating voltage	200 kV
Source size	0.1 nm
Oversampling	4

would increase the simulation time dramatically. Fig. 2(c) is generated in 0.15 s (nearly 'real-time') from our kinematic simulation software with 512×512 pixels on the same computer. The same Gaussian width of 0.8 Angstrom is applied in both cases. Fig. 2(d) is the line profile indicated by the yellow rectangular in (b) and (c). The dashed line and solid line are scaled at the second peak indicated by the arrow in Fig. 2(d). To the first order approximation, the atom column positions and the relative peak intensity are comparable between two simulations. For small clusters, this is due to the balance between the natural broadening effect of the probe, the focusing effect of the atomic potential and the de-channeling effect of the atomic vibration (Aveyard et al., 2014). This results in an effective monotonic increase of scattered electron intensity with the number of atoms within the atomic column when the number of atoms is small (Young et al., 2008; Li et al., 2008), hence it can be modeled by an effective kinematic model. This property has been used in discrete tomography (Van Aert et al., 2011) and also by the current approach.

4.1.2. Multiply twinned structure

Our simple model is particularly effective for multiply twinned nanoparticles as the image contrast is dominated by the Moire

effect due to overlapping single crystalline motifs in the twinned nanoparticles. The other dynamical scattering effect is also minimized because of the small effective size of the single crystalline materials, although our image simulation will not show the 'top–bottom' effect which is characteristic of the dynamical scattering (Howie and Basinski, 1968).

Multiply twinned structures (icosahedron and decahedron) are widely reported in nanoparticles of the face centered cubic metals, such as Au, Ag and Pd (Li et al., 2008; Marks, 1984, 1994; Elechiguerra et al., 2006; Koga and Sugawara, 2003; Wang and Palmer, 2012). These structures compose of slightly distorted face centered cubic subunits. Fig. 3 shows both multislice simulation and kinematic simulation of an isolated Au nanoparticle comprising 923 atoms and with a magic number icosahedral structure, from ⟨2 1 1⟩ and ⟨1 1 0⟩ directions, respectively. All other parameters used are the same as in the previous case in Fig. 2. It is clear that the overall shape and the atom column positions have been well reproduced using the kinematic simulation approach alone, though some departures in detailed line intensity profiles are apparent in Fig. 3(d) and (h), highlighting the importance of the multiple electron scattering effect in this multiply twinning nanoparticle if quantitative analysis is of interest. For this non-trivial case, we can also see that our image simulation is much closer to the multislice result than the information that can be provided by the projected image of the hard-ball model of the atomic structure.

4.2. Orientation dependence

The efficient modeling capability of our simulation package is most useful in investigation of the orientation dependence of the HAADF-STEM images of nanoparticles. In the literature, many simulations of the orientation dependence are reported with several degrees increment in orientation (Koga and Sugawara, 2003; Wang and Palmer, 2012; Kirkland et al., 1991), which is not detailed enough for practical orientation determination as it could lead to missing the fine features of the orientation dependence. In Fig. 4,
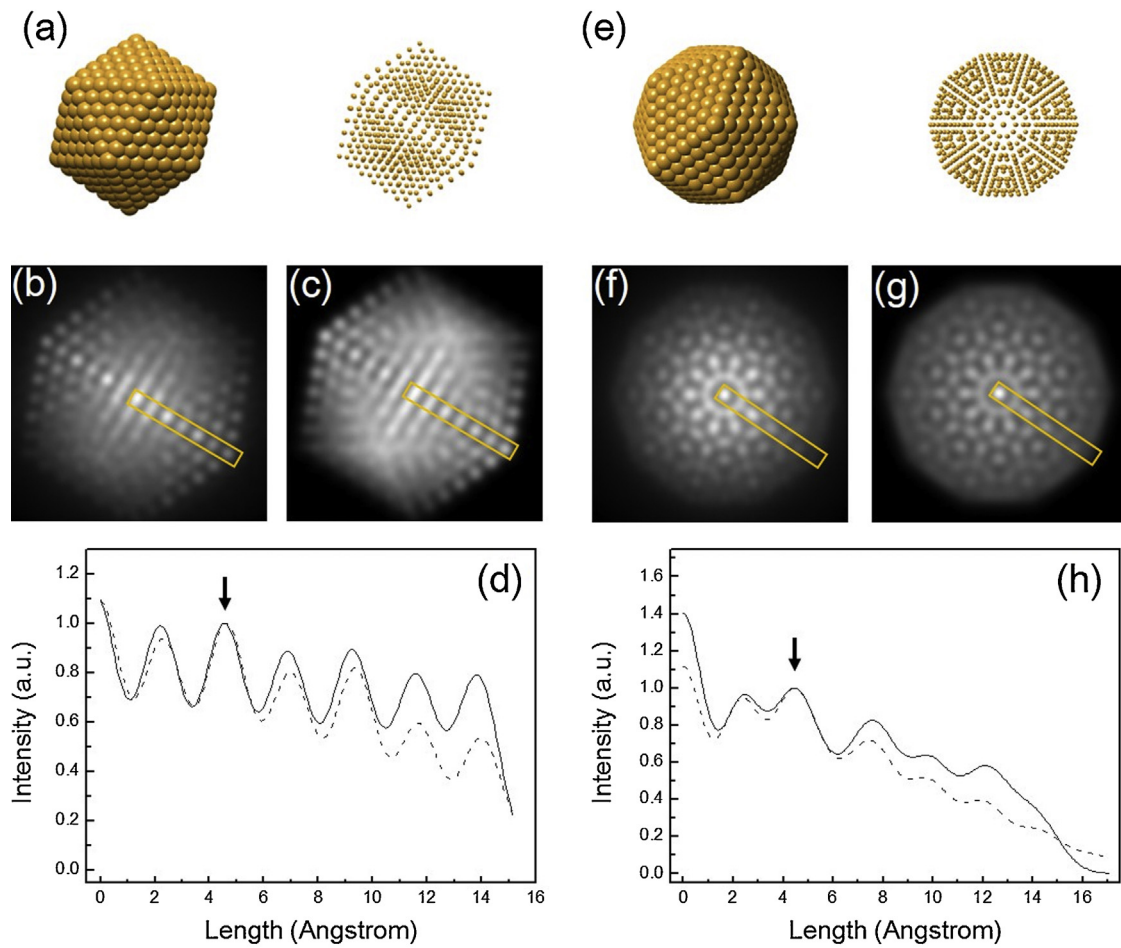
Fig. 3. (a, e) The hard-ball models for an icosahedron containing 923 atoms from ⟨2 1 1⟩ and ⟨1 1 0⟩ orientations. Multislice simulations (b, f) and kinematic simulations (c, g). (d, h) The line profiles indicated by the yellow rectangular in (b, c) and (f, g), respectively. The dashed lines are from the multislice simulations while the solid lines are from the kinematic simulations. The line profiles are averaged over 15 pixels. (For interpretation of the references to color in this figure legend, the reader is referred to the web version of this article.)

we use this software to generate a series of images for the same icosahedron model containing 923 atoms from ⟨1 1 0⟩ tilting up to 4° off, in step of 1°. It shows clearly that the pattern varies a great deal, e.g., the central ring disappears at 2° off the ⟨1 1 0⟩ zone axis in Fig. 4(b3). In practice, the particle orientation search is a search in the two dimensional angular space. Using this software, the fast simulation speed enables us to identify, for example, the exact orientation of a given experimental image of the multiply twinned
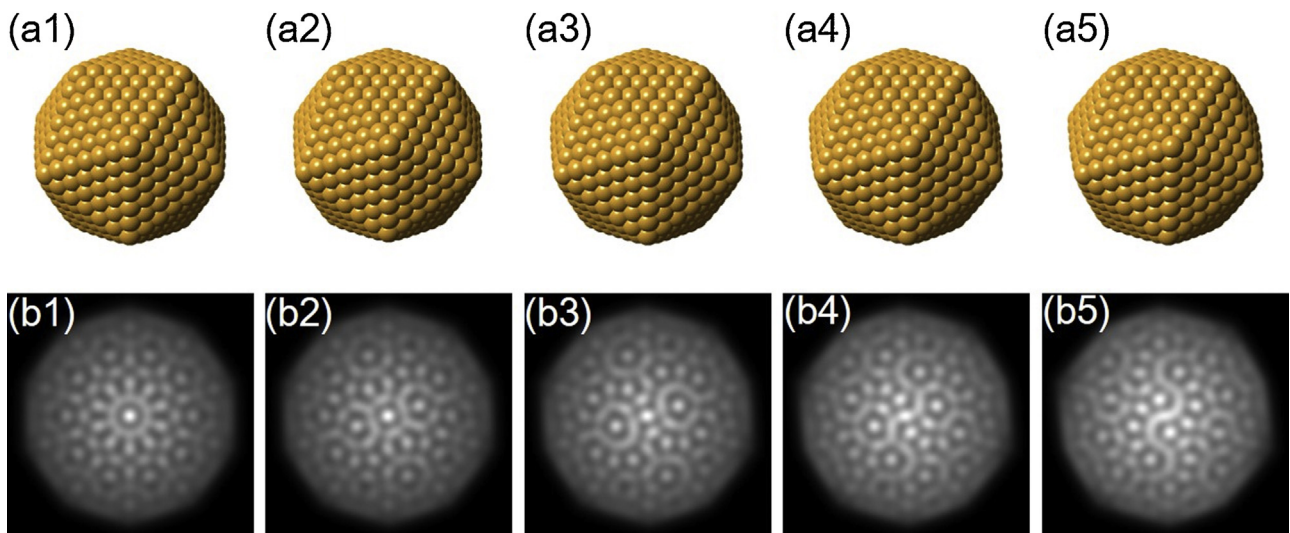

Fig. 4. Kinematic simulation of an icosahedral nanoparticle containing 923 atoms. (a1–a5) Hardball models of the nanoparticles tilted from ⟨1 1 0⟩ zone axis to 4° off, with increment of 1° (0°, 1°, 2°, 3° and 4°). (b1–b5) simulated HAADF-STEM images of the nanoparticle in corresponding tilting angles.
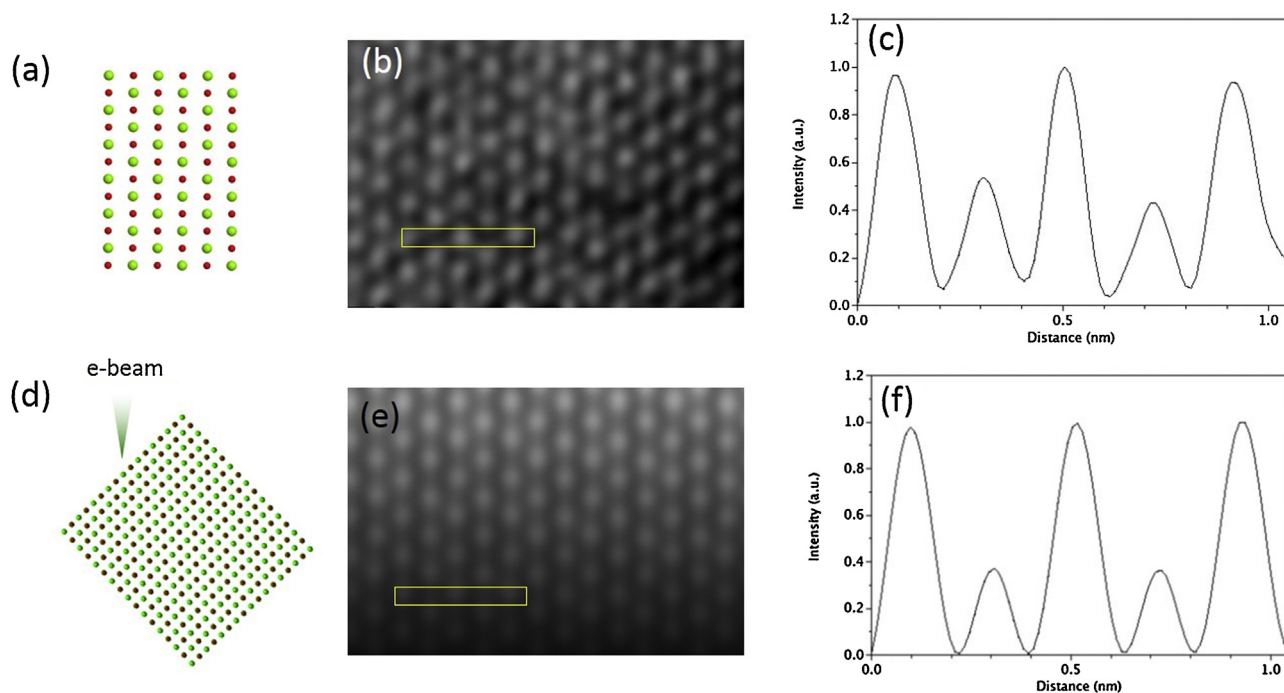
Fig. 5. Comparison between experimental image (top) and kinematic simulation (bottom) image of MgO at ⟨1 1 0⟩. (a, d) The hard-ball model of MgO where green balls are the Mg atomic columns and red balls are the O atomic columns. (c, f) The line profiled indicated by the yellow rectangular in (b, e). The experimental image was Gaussian blurred with 4 pixels to remove the noise and the line profiles are 10 pixels wide. The line profiles are normalized. (For interpretation of the references to color in this figure legend, the reader is referred to the web version of this article.)

nanoparticles by systematically tilting the model nanoparticle and generate the associated images in real time. This is of considerable practical value as the pattern recognition required in orientation determination is still best done using human brain rather than the computer simulation although the latter is catching up fast.

4.3. Z-contrast imaging and simulation

When there is more than one element in a nanoparticle, it can lead to Z-contrast between elements, as heavier elements have a stronger ability to scatter electrons. To illustrate this contrast, MgO nanometer sized cubes with (1 0 0) face exposed were prepared by burning magnesium ribbon in air. A 200 kV JEOL 2100f STEM equipped with a CEOS probe lens aberration corrector and an ADF detector with inner and outer collection angle of 55 and 148 mrad was employed to image the MgO cubes. MgO (1 0 0) was tilted to the ⟨1 1 0⟩ direction and the experimental image is shown in Fig. 5(b). At this direction, the Mg and O columns are alternatively separated, see Fig. 5(a). The line profile in Fig. 5(c), indicated by the yellow rectangular in Fig. 5(b), shows peaks with alternative higher and lower intensity peaks. Fig. 5(e) is the kinematic simulated image using this software with a cubic MgO atom model which illustrates the similar pattern as in Fig. 5(b). In particular, the line profiles in Fig. 5(c) and (f) show a close correlation of high and low intensity peaks in both experimental and simulated images.

5. Conclusion

To conclude, in this paper, an efficient, versatile and user-friendly software for kinematic HAADF-STEM simulation is described. The validity of the assumption of kinematic electron scattering is demonstrated in nanoparticles of Au and MgO. The software enables users to compute HAADF-STEM images in "real time" on a standard desktop computer. It allows users to treat multiple elements within particles to examine the effect of elemental

contrast; it also allows users to display Fast Fourier transform of images together with hardball models for visualization of projection of nanoparticles. The output of data provides the starting point of the multislice simulation if one wants to study multiple electron scattering effects or surface photon effects by comparing the absolute intensity (Li et al., 2008; Aveyard et al., 2014). This software can potentially be incorporated with automatic image recognition to enable easier searching for a particular nanoparticle structure (Logsdail et al., 2012; Flores et al., 2003) and help with sample tilting under STEM mode.

References

Arfken, G., 1985. Mathematical Methods for Physicists, 3rd ed. Academic Press, Orlando.

Aveyard, R., Ferrando, R., Johnston, R.L., Yuan, J., 2014. Modelling nanoscale inhomogeneities for quantitative HAADF STEM imaging. Phys. Rev. Lett. 113, 075501.

Chen, C.C., Zhu, C., White, E.R., Chiu, C.Y., Scott, M.C., Regan, B.C., Marks, L.D., Huang, Y., Miao, J., 2013. Three-dimensional imaging of dislocations in a nanoparticle at atomic resolution. Nature 496, 74.

Curley, B.C., Johnston, R.L., Young, N.P., Li, Z.Y., Di Vece, M., Palmer, R.E., Bleloch, A.L., 2007. Combining theory and experiment to characterize the atomic structures of surface-deposited Au$_{309}$ clusters. J. Phys. Chem. C 111, 17846.

Dwyer, C., 2010. Simulation of scanning transmission electron microscope images on desktop computers. Ultramicroscopy 110, 195.

Elechiguerra, J.L., Reyes-Gadga, J., Yacaman, M.J., 2006. The role of twinning in shape evolution of anisotropic noble metal nanostructures. J. Mater. Chem. 16, 3906–3919.

Flores, A.B., Robles, L.A., Arias, M.O., Ascencio, J.A., 2003. Small metal nanoparticle recognition using digital image analysis and high resolution electron microscopy. Micron 34, 109.

Galindo, P., Pizarro, J., Rosenauer, A., Yáñez, A., Guerrero, E., Molina, S.I., 2008. HAADF-STEM image simulation of large scale nanostructures. EMC 2008 1, 111.

Grillo, V., Rotunno, E., 2013. STEM_CELL: a software tool for electron microscopy. Part I – simulations. Ultramicroscopy 125, 97.

Haider, M., Rose, H., Uhlemann, S., Schwan, E., Kabius, B., Urban, K., 1998. A spherical-aberration-corrected 200 kV transmission electron microscope. Ultramicroscopy 75, 53.

Han, Y., He, D.S., Liu, Y., Xie, S., Tsukuda, T., Li, Z.Y., 2012. Size and shape of nanoclusters: single-shot imaging approach. Small 8, 2361.

Hartel, P., Rose, H., Dinges, C., 1996. Conditions and reasons for incoherent imaging in STEM. Ultramicroscopy 63, 93.

He, D.S., Li, Z.Y., 2014. A practical approach to quantify the ADF detector in STEM. J. Phys. Conf. Ser. 522, 012017.

Howie, A., Basinski, Z.S., 1968. Approximations of the dynamical theory of diffraction contrast. Philos. Mag. 17, 1039–1063.

HREM Research Inc., www.hremresearch.com

Jesson, D.E., Pennycook, S.J., 1995. Incoherent imaging of crystals using thermally scattered electrons. Proc. R. Soc. Lond. Ser. A: Math. Phys. Sci. 449, 273.

Katz-Boon, H., Rossouw, C.J., Dwyer, C., Etheridge, J., 2013. Rapid measurement of nanoparticle thickness profiles. Ultramicroscopy 124, 61.

Kauko, H., Grieb, T., Bjørge, R., Schowalter, M., Munshi, A.M., Weman, H., Rosenauer, A., van Helvoort, A.T.J., 2012. Compositional characterization of GaAs/GaAsSb nanowires by quantitative HAADF-STEM. Micron 44, 254.

Kirkland, E.J., 2010. Advanced Computing in Electron Microscopy, 2nd ed. Springer.

Kirkland, A.I., Jefferson, D.A., Tang, D., Edwards, P.P., 1991. High-resolution image simulations of small metal particles. Proc. R. Soc. Lond. Ser. A: Math. Phys. Sci. 434, 279–296.

Koch, C., (PhD thesis) 2002. Determination of Core Structure Periodicity and Point Defect Density Along Dislocations. Arizona State University.

Koga, K., Sugawara, K., 2003. Population statistics of gold nanoparticle morphologies: direct determination by HREM observations. Surf. Sci. 529, 23–25.

LeBeau, J.M., Findlay, S.D., Allen, L.J., Stemmer, S., 2008. Quantitative atomic resolution scanning transmission electron microscopy. Phys. Rev. Lett. 100, 206101.

LeBeau, J.M., Findlay, S.D., Allen, L.J., Stemmer, S., 2010. Standardless atom counting in scanning transmission electron microscopy. Nano Lett. 10, 4405.

Li, Z.Y., Young, N.P., Di Vece, M., Palomba, S., Palmer, R.E., Bleloch, A.L., Curley, B.C., Johnston, R.L., Jiang, J., Yuan, J., 2008. Three-dimensional atomic-scale structure of size-selected gold nanoclusters. Nature 451, 46.

Logsdail, A.J., Li, Z.Y., Johnston, R.L., 2012. Development and optimization of a novel genetic algorithm for identifying nanoclusters from scanning transmission electron microscopy images. J. Comput. Chem. 33, 391.

Marks, L.D., 1984. Surface structure and energetics of multiply twinned particles. Philos. Mag. A 49, 81.

Marks, L.D., 1994. Experimental studies of small particle structures. Rep. Prog. Phys. 57, 603.

Martin, T.P., 1996. Shells of atoms. Phys. Rep. 273, 199–241.

Nellist, P.D., Pennycook, S.J., 1999. Incoherent imaging using dynamically scattered coherent electrons. Ultramicroscopy 78, 111.

Nellist, P.D., Pennycook, S.J., 2000. The principles and interpretation of annular dark-field Z-contrast imaging. Adv. Imaging Electron Phys. 113, 147.

Nellist, P.D., Chisholm, M.F., Dellby, N., Krivanek, O.L., Murfitt, M.F., Szilagyi, Z.S., Lupini, A.R., Borisevich, A., Sides Jr., W.H., Pennycook, S.J., 2004. Direct sub-Angstrom imaging of a crystal lattice. Science 305, 1741.

Nellist, P.D., Lozano-Perez, S., Ozkaya, D., 2010. Towards quantitative analysis of core–shell catalyst nanoparticles by aberration corrected high angle annular dark field STEM and EDX. J. Phys. Conf. Ser. 241, 012067.

Scott, M.C., Chen, C.C., Mecklenburg, M., Zhu, C., Xu, R., Ercius, P., Dahmen, U., Regan, B.C., Miao, J., 2012. Electron tomography at 2.4-Angstrom resolution. Nature 483, 444.

Van Aert, S., Batenburg, K.J., Rossell, M.D., Erni, R., Van Tendeloo, G., 2011. Three-dimensional atomic imaging of crystalline nanoparticles. Nature 470, 374.

Van Aert, S., De Backer, A., Martinez, G.T., Goris, B., Bals, S., Van Tendeloo, G., 2013. Procedure to count atoms with trustworthy single-atom sensitivity. Phys. Rev. B 171, 064107.

Wang, Z.L., 2000. Transmission electron microscopy of shape-controlled nanocrystals and their assemblies. J. Phys. Chem. B 104, 1153.

Wang, Z.W., Palmer, R.E., 2012. Determination of the ground-state atomic structures of size-selected Au nanoclusters by electron-beam-induced transformation. Phys. Rev. Lett. 108, 245502.

Wang, Z.W., Li, Z.Y., Park, S.J., Abdela, A., Tang, D., Palmer, R.E., 2011. Quantitative Z-contrast imaging in the scanning transmission electron microscope with size-selected clusters. Phys. Rev. B 84, 073408.

Young, N.P., Li, Z.Y., Chen, Y., Palomba, S., Di Vece, M., Palmer, R.E., 2008. Weighing supported nanoparticles: size-selected clusters as mass standards in nanometrology. Phys. Rev. Lett. 101, 246103.